Journal of Materials Chemistry A

RSC Publishing

PAPER

View Article Online
View Journal | View Issue

Cite this: J. Mater. Chem. A, 2013, 1, 11802

Air-stable inverted structure of hybrid solar cells using a cesium-doped ZnO electron transport layer prepared by a sol–gel process

Seungchul Kwon,†[a] Kyung-Geun Lim,†[b] Myungsun Shim,[c] Hong Chul Moon,[a] Jicheol Park,[a] Gumhye Jeon,[a] Jihyun Shin,[a] Kilwon Cho,[c] Tae-Woo Lee*[b] and Jin Kon Kim*[a]

We have developed an air-stable inverted structure of poly(3-hexylthiophene) (P3HT) : cadmium selenide (CdSe) hybrid solar cells using a cesium-doped ZnO (ZnO:Cs) electron transport layer. The ZnO:Cs layer was simply prepared at low temperature by the sol–gel process using a ZnO solution containing cesium carbonate (Cs_2CO_3). With increasing Cs-doping concentration, the conduction band edge of ZnO is decreased, as confirmed by scanning Kelvin probe microscopy. The energy level of ZnO:Cs is effective for electron transport from CdSe. Consequently, the power conversion efficiency (PCE) of the inverted P3HT : CdSe hybrid solar cells using the ZnO:Cs electron transport layer is 1.14%, which is significantly improved over that (0.43%) of another device without Cs. X-ray photoelectron spectroscopy analysis revealed that the amount of CdSe on the substrate (or the bottom surface) is larger compared with the air (or top) surface regardless of the P3HT : CdSe weight ratio. The vertically inhomogeneous distribution of CdSe in the hybrid solar cells gives better charge transport from CdSe to ZnO:Cs in the inverted structure of the device compared with that in the normal structure. As a result, the inverted hybrid solar cell consisting of 1 : 4 (wt/wt) P3HT : CdSe shows the best efficiency, while the best efficiency of a normal hybrid solar cell is achieved at 1 : 9 (wt/wt) P3HT : CdSe.

Received 21st June 2013
Accepted 1st August 2013

DOI: 10.1039/c3ta12425h

www.rsc.org/MaterialsA

Introduction

Organic-based photovoltaic cells have been attracting immense attention as next-generation solar cells due to their excellent solution processability, low cost, and large area fabrication. Particularly, inorganic nanocrystals combined with an organic semiconducting material (electron donor) are of great interest for use as a light-absorbing electron acceptor, because of their efficient charge transport,[1] tunable band gap depending on size and shape,[2] high absorption coefficient,[3] good stability of nanostructures,[4] and efficient charge transfer from an organic donor with S atoms (for instance, poly(3-hexylthiophene) (P3HT)) to inorganic nanocrystals due to strong coordination interaction between S atoms in the organic donor and inorganic nanocrystals.[5] Especially, elongated nanostructures of inorganic nanocrystals such as nanorods[1] and tetrapods[6] have been widely used for hybrid solar cells due to the effective electron transport. Recently, a significant improvement in the device performance has been achieved using PbS,[7] CdS,[8] and CdTe.[9] Additionally, ternary $Cd_xHg_{1-x}Te$[10–12] and quaternary $Cu_2ZnSnSe_4$ nanocrystals[13] have been explored for hybrid solar cells because of their low-toxicity, appropriate band gap (1.0–1.5 eV), and relatively abundant component elements.

Conventional hybrid solar cells (hereafter referred to as normal hybrid solar cells) typically consist of an organic–inorganic hybrid thin film sandwiched between poly(3,4-ethylenedioxylthiophene):poly(styrenesulfonate) (PEDOT:PSS) as an anodic buffer layer on a transparent anode and a metal cathode with a low work function.[1] Acidic and hygroscopic PEDOT:PSS, however, causes a stability problem in normal hybrid solar cells.[14] Accordingly, the development of the inverted structure of a device without having PEDOT:PSS is essential for achieving better device stability.[15–17]

The efficiency of an inverted hybrid solar cell is significantly affected by the morphology of the active layer and the materials of anodic and cathodic buffer layers. Even though the inverted hybrid solar cells use inorganic nanocrystals as the bottom contact unlike the normal hybrid solar cells,[18] the morphology of the active layer at the top and bottom contacts in the hybrid solar cells has not been studied in detail. Moreover, anodic buffer layers based on metal oxides such as

[a]National Creative Research Center for Block Copolymer Self-Assembly, Department of Chemical Engineering and Polymer Research Institute, Pohang University of Science and Technology, Gyungbuk 790-784, Korea. E-mail: twlee@postech.ac.kr; jkkim@postech.ac.kr; Fax: +82 279 8298

[b]Department of Materials Science and Engineering, Pohang University of Science and Technology, Gyungbuk 790-784, Korea

[c]Department of Chemical Engineering and Polymer Research Institute, Pohang University of Science and Technology, Gyungbuk 790-784, Korea

† S. Kwon and K.-G. Lim contributed equally to this work.

TiO_2 and ZnO having solution processability, environmental stability, and high electron mobility have been recently employed at the active layer/cathode interface of the inverted hybrid solar cells.[15–17] However, the sol–gel process for preparing TiO_2 films requires high annealing temperature (350–500 °C), which is unsuitable for flexible device applications.[15,16] Although TiO_2 nanoparticles could be used for the solution process at room temperature, the nanoparticles are not stable for the solution process without appropriate ligands.[19] For another inverted device using sol–gel-derived ZnO prepared at relatively low temperature (~200 °C), the deposition of an additional fullerene (C_{60}) buffer layer on ZnO is needed for optimal band alignment with an inorganic acceptor material (CdTe) because the conduction band edge of ZnO is considerably lower than the lowest unoccupied molecular orbital (LUMO) of inorganic nanocrystals.[17]

To match the LUMO of CdSe nanorods, in this study, we employed a cesium-doped ZnO (ZnO:Cs) electron transport layer. ZnO:Cs thin films are fabricated by the sol–gel process at low temperature (~200 °C) of ZnO solution containing cesium carbonate (Cs_2CO_3). X-ray photoelectron spectroscopy (XPS) analysis revealed that the CdSe concentration in the P3HT : CdSe hybrid thin film is higher on the bottom surface (or the substrate) compared with that on the top (or air) surface. The vertically inhomogeneous distribution of CdSe through the film thickness becomes a favorable morphology for inverted hybrid solar cells. Due to an efficient electron transport from CdSe to ZnO:Cs on the ITO glass substrate, the optimum concentration of CdSe relative to P3HT in the P3HT : CdSe inverted hybrid solar cell for the best device performance was 1 : 4 wt/wt P3HT : CdSe, which is much smaller than that (1 : 9 wt/wt P3HT : CdSe) of normal hybrid solar cells.

Experimental section

Synthesis of CdSe nanorods

Cadmium oxide (CdO, ≥99.99%), trioctylphosphine oxide (TOPO, technical-grade, 90%) and trioctylphosphine (TOP, 97%) were purchased from Sigma-Aldrich. Octylphosphonic acid (OPA) was purchased from PCI Synthesis. All reagents and chemicals were used without further purification. CdSe nanorods were synthesized according to the literature.[20] 0.1284 g of CdO (1.0 mmol), 0.3923 g of OPA (2.0 mmol), and 2.0 g of TOPO were loaded into a flask and heated to 310 °C under a nitrogen flow to dissolve CdO in the OPA–TOPO solution. After a transparent solution was obtained, it was cooled down to 120 °C and kept under vacuum for 2 h. The solution was heated to 320 °C and then the TOP–selenium complex (0.1184 g of selenium (1.5 mmol) in 1.0 g of TOP) was quickly injected into the flask. This solution was kept at 320 °C for 20 min and the reaction was stopped by removing the heating mantle. Hexane (10 ml) was added to the flask to dissolve the nanorods at 50 °C. Methanol (80 ml) was used to separate the CdSe nanorods from organic surfactants by centrifugation and decantation three times, and then the solution was dried and stored in a vacuum.

Pyridine treatment of CdSe nanorods

CdSe nanorods were added to anhydrous pyridine (30 ml) and refluxed at 120 °C for 24 h under a nitrogen flow. After pyridine treatment, the CdSe nanorods were centrifuged with hexane (120 ml) and redissolved in chloroform (10 ml). The CdSe–chloroform solution was sonicated for 30 min and then filtrated using a 1 μm PTFE filter. The filtrated solution was dried and kept under vacuum.

Synthesis of P3HT

Allyl-end functionalized P3HT (the number average molecular weight = 29 000 and the polydispersity index = 1.20) was synthesized in our laboratory[21,22] and used without further purification.

Preparation of ZnO:Cs solution

0.46 M zinc acetate dihydrate (99.999%, Aldrich), 0.46 M ethanolamine (≥99.5%, Aldrich), and cesium carbonate (Cs_2CO_3, 99.995%, Aldrich) were dissolved in 2-methoxyethanol (anhydrous, 99.8%, Sigma-Aldrich) and vigorously stirred at 70 °C for 24 h in air.

Fabrication of inverted P3HT : CdSe hybrid solar cells

All devices were fabricated on an indium-tin oxide (ITO)-coated glass. The ITO glass was sequentially cleaned using acetone, ethanol, Mucasol detergent diluted in deionized water, acetone, and ethanol in an ultrasonic bath. Next, the ITO glass was spin-coated with ZnO:Cs sol at 2000 rpm for 60 s and annealed at 200 °C for 30 min in air. The P3HT and CdSe (total 33 mg) were mixed in 1,2-dichlorobenzene (DCB, anhydrous, 99%, Sigma-Aldrich, 0.94 ml) and pyridine (anhydrous, 99.8%, Sigma-Aldrich, 0.06 ml) and stirred at 50 °C for 12 h. The solution was spin-coated onto the ZnO:Cs-coated ITO glass substrates at 800 rpm for 90 s, annealed at 120 °C for 20 min, and then transferred to a high-vacuum chamber for MoO_3 (7 nm)/Ag (100 nm) deposition at rates of 0.3 Å s^{-1} and 0.5 Å s^{-1}, respectively, on top of the P3HT : CdSe blend films. The active area was 0.06 cm^2.

Characterizations

The shape and size of CdSe nanorods were investigated by transmission electron microscopy (TEM) (JEOL JEM-2100F). The Cd/S atomic ratio was characterized by XPS (VG ESCALAB 220 iXL system with a mono-chromated Al Kα (1486.6 eV) X-ray source). The optical properties of the CdSe nanorod film and P3HT : CdSe thin films were characterized using a Cary 5000 UV-Vis-NIR spectrophotometer. The surface potential shift of ZnO:Cs films was obtained by scanning Kelvin probe microscopy (SKPM) (Kelvin Probe System SKP5050). Atomic force microscopy (AFM) (Digital Instruments D3000) in the tapping mode with silicon nitride tips on cantilevers (Nanoprobe) was used to characterize the surface morphology of ZnO:Cs thin films with various Cs/Zn molar ratios.

Results and discussion

Fig. 1(a) shows a schematic for the device structure of inverted hybrid solar cells based on P3HT and CdSe. Fig. 1(b) and (c) show the chemical structure of the electron donor (P3HT) and the TEM image of the electron acceptor (CdSe nanorods with a diameter of 5–6 nm and an average length of ~27 nm), respectively. The inset of Fig. 1(c) shows the histogram of the CdSe nanorod length. In this inverted structure, ITO and Ag were used as the cathode and the anode, respectively. High-work-function MoO_3 was deposited on top of the P3HT : CdSe films as a hole transport layer, while the ZnO:Cs thin film with various Cs/Zn molar ratios was used for an electron transport layer on the ITO glass substrate. The P3HT and CdSe mainly absorb visible light, resulting in the generation of photo-excited excitons (electron–hole pairs). After exciton diffusion to the interface of P3HT and CdSe, the electrons and holes are separated into CdSe and P3HT, respectively, and transported toward each electrode.

The plots of the current density–voltage (J–V) characteristics measured under the solar-simulated air mass (AM) 1.5 G illumination at an intensity of 100 mW cm^{-2} for the inverted P3HT : CdSe (1 : 4 weight ratio) hybrid solar cells using ZnO:Cs electron transport layers with various Cs/Zn molar ratios are shown in Fig. 2(a). The corresponding characteristics of the inverted hybrid solar cells depending on the Cs/Zn molar ratios are summarized in Table 1. The inverted hybrid solar cell using pristine ZnO without Cs shows an open circuit voltage (V_{OC}) of 0.521 V, a short circuit current density (J_{SC}) of 2.5 mA cm^{-2}, and a fill factor (FF) of 32.7%; thus, the power conversion efficiency (PCE) is 0.43%. A considerably improved performance of the inverted hybrid solar cell is obtained when the Cs/Zn molar ratio is 0.094: a V_{OC} of 0.633 V, a J_{SC} of 4.7 mA cm^{-2}, an FF of 38.4%, and a PCE of 1.14%. Particularly, the V_{OC} and J_{SC} of the device are significantly enhanced (Fig. 2(b)). One possible reason for the increased performance of the devices using ZnO:Cs is the reduction in series resistance (R_S) including contact resistance at the ZnO:Cs/P3HT : CdSe interface.[23] To reveal the J_{SC} enhancement, the R_S of inverted hybrid solar cells depending on the Cs/Zn molar ratio was extracted from the J–V characteristics (Fig. 2(c) and Table 1). We clearly see a reduction in R_S for the devices using the ZnO:Cs layer. The device using ZnO:Cs with a Cs/Zn molar ratio of 0.094 shows an R_S of 64.2 Ω cm^2, which is almost half of the R_S of the device using pristine ZnO (127 Ω cm^2). The reduced R_S is favorable for electron

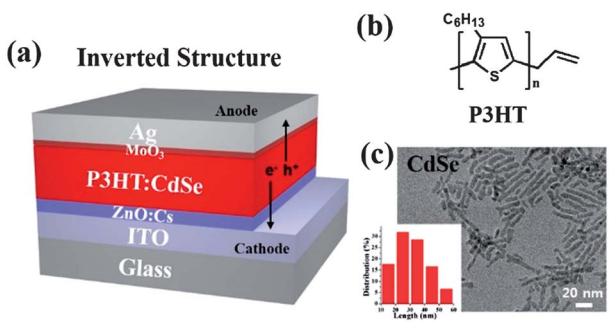

Fig. 1 (a) Device illustration of the inverted P3HT : CdSe hybrid solar cell. (b) The chemical structure of P3HT and (c) the transmission electron microscopy (TEM) image of CdSe nanorods. The inset is the histogram of the CdSe nanorod length.

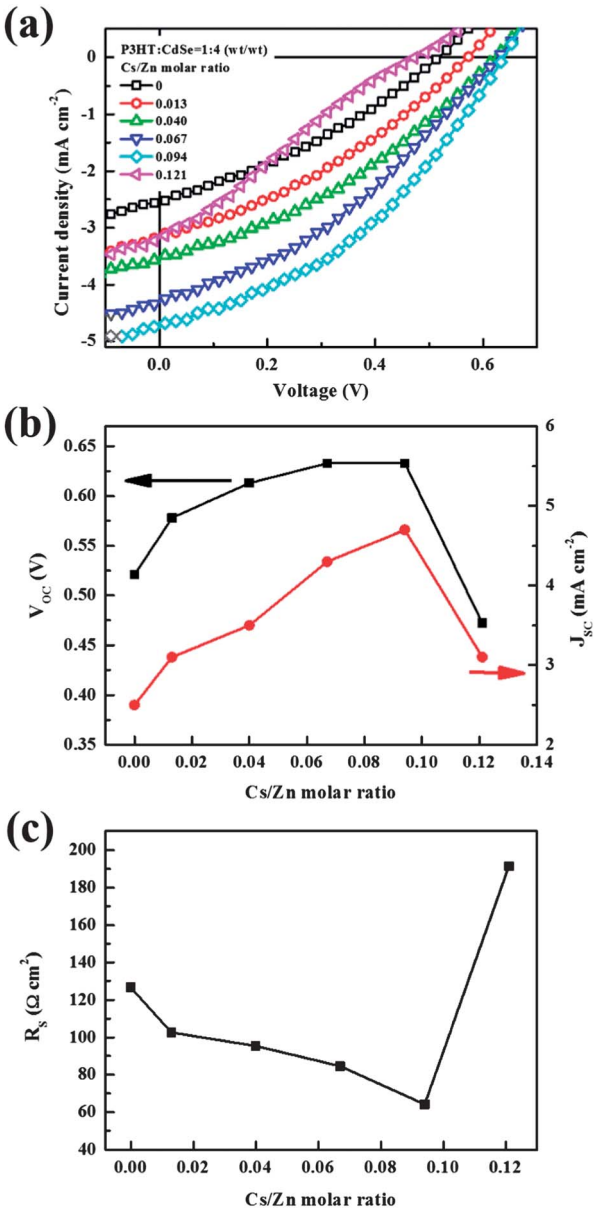

Fig. 2 (a) J–V curves, (b) J_{SC} and V_{OC}, and (c) series resistance (R_S) of inverted P3HT : CdSe hybrid solar cells with various amounts of Cs in the ZnO:Cs layer.

Table 1 Performance of the inverted devices based on P3HT : CdSe blends using the ZnO:Cs electron transport layer with various amounts of Cs

Cs/Zn molar ratio	V_{OC} (V)	J_{SC} (mA cm^{-2})	FF (%)	R_S (Ω cm^2)	PCE (%)
0	0.521	2.5	32.7	127	0.43
0.013	0.578	3.1	33.3	103	0.60
0.04	0.613	3.5	35.2	95.4	0.76
0.067	0.633	4.3	34.1	84.6	0.93
0.094	0.633	4.7	38.4	64.2	1.14
0.121	0.472	3.1	24.8	191	0.36

extraction from CdSe to the ZnO:Cs layer. However, when the Cs/Zn molar ratio is further increased to 0.121, the PCE becomes poorer because of the low J_{SC} (3.1 mA cm^{-2}) and low V_{OC} (0.472 V).

To investigate the poor device performance at a Cs/Zn molar ratio of 0.121, the surface morphology of the ZnO:Cs films was investigated by AFM. As shown in Fig. 3(a)–(c), ZnO:Cs thin films with a Cs/Zn molar ratio up to 0.094 show smaller root-mean-squared (RMS) roughness (~2.5 nm) on ITO glass substrates. However, as shown in Fig. 3(d), ZnO:Cs with a Cs/Zn molar ratio of 0.121 shows a very rough surface with an RMS roughness of 6.16 nm. The roughened surface morphology may be attributed to the phase separation of ZnO and Cs_2CO_3 after annealing on the ITO glass because of large amounts of Cs_2CO_3. Once Cs_2CO_3 is aggregated, it acts as an insulator. When the surface becomes rough, the leakage current occurs through the peaks of the ZnO:Cs layer, leading to a poor FF. Also, the aggregated Cs_2CO_3 domains result in high R_S at the interface between ZnO:Cs and CdSe. The low V_{OC} of a device with a higher Cs/Zn molar ratio of 0.121 might be attributed to increased leakage current and density of the trap sites, resulting in trap-assisted recombination on the rough ZnO:Cs surface.[24,25]

To verify the V_{OC} enhancement of the device using the ZnO:Cs electron transport layer, the surface potential shift of ZnO:Cs films depending on the Cs-doping concentration was measured by SKPM. As shown in Fig. 4(a), the surface potential shift of ZnO:Cs is gradually decreased depending on the Cs/Zn molar ratio. Therefore, the conduction band edge of ZnO:Cs shifts upward to match the LUMO of CdSe with increasing Cs/Zn molar ratio. The V_{OC} is generally affected by the conduction band edge of the electron transport layer.[26,27] As a result, the V_{OC} of the device increases with increasing Cs/Zn molar ratio at lower Cs/Zn molar ratios. Especially, the surface potential at a Cs/Zn molar ratio of 0.067 was shifted by −0.17 V; thus, the V_{OC} reaches the maximum (0.633 V). The conduction band edge of ZnO is known to be 4.2 eV,[28] while the LUMO of pyridine-treated CdSe is known to be 4.0 eV.[29] Thus, the conduction band edge of ZnO:Cs with a Cs/Zn molar ratio of 0.067 is pinned to the LUMO of CdSe, as shown schematically in Fig. 4(b). Thus, the increase in V_{OC} is attributed to the decrease of the conduction band edge of ZnO:Cs to match the LUMO of CdSe nanorods.

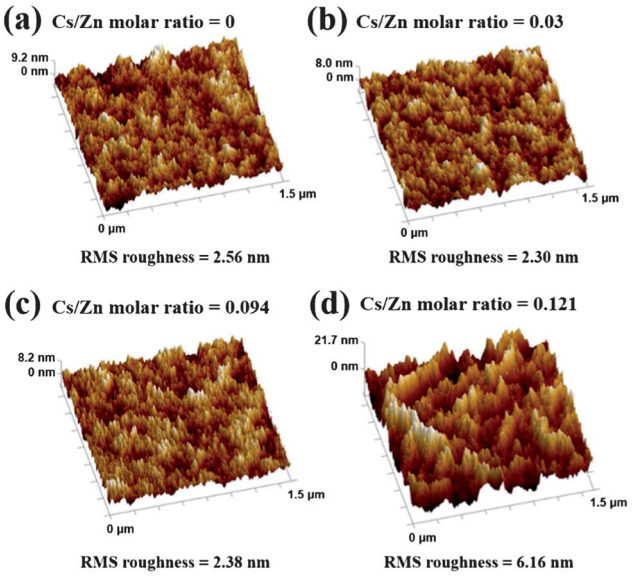

Fig. 3 AFM height images of (a) pristine ZnO, (b) ZnO:Cs (Cs/Zn molar ratio = 0.030), (c) ZnO:Cs (Cs/Zn molar ratio = 0.094), and (d) ZnO:Cs (Cs/Zn molar ratio = 0.121).

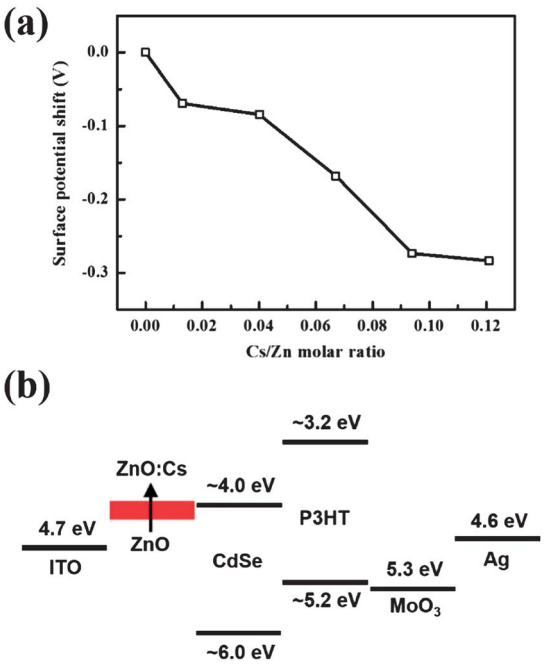

Fig. 4 (a) Surface potential of ZnO as a function of the Cs/Zn molar ratio measured by scanning Kevin probe microscopy (SKPM) and (b) the schematic energy level diagram for the materials used in the device.

The device performance was also studied as a function of the P3HT : CdSe weight ratio using the ZnO:Cs thin film at a given Cs/Zn molar ratio of 0.094. Fig. 5(a) indicates that the performance of the inverted hybrid solar cells was greatly influenced by the weight ratio of P3HT to CdSe. With the increase in the CdSe concentration, the J_{SC} and V_{OC} of the device initially increased up to 1 : 4 (wt/wt) P3HT : CdSe, and then decreased. The maximum PCE was 1.14% at 1 : 4 (wt/wt) P3HT : CdSe. Generally, in normal hybrid solar cells, the increase in the CdSe concentration in the active layer generates more electron pathways to the top contact.[18] The performance of inverted hybrid solar cells is, however, optimized at 1 : 4 (wt/wt) P3HT : CdSe, which means that even low CdSe concentrations in the inverted structure create sufficient percolation pathways to the bottom contact for efficient electron transport. In addition, the increased P3HT concentration in the active layer up to 1 : 4 (wt/wt) P3HT : CdSe contributes to more light absorption (Fig. 5(c)), resulting in favorable percolation pathways for hole transport. The contribution of P3HT and CdSe to generate photocurrent was investigated using the incident photon-to-electron conversion efficiency (IPCE) spectra of the inverted hybrid solar cells with various P3HT : CdSe weight ratios. As shown in Fig. 5(b), the maximum IPCE of the device with 1 : 4 (wt/wt) P3HT : CdSe reached 39% with the absorption peak at 525 nm, which means that in the

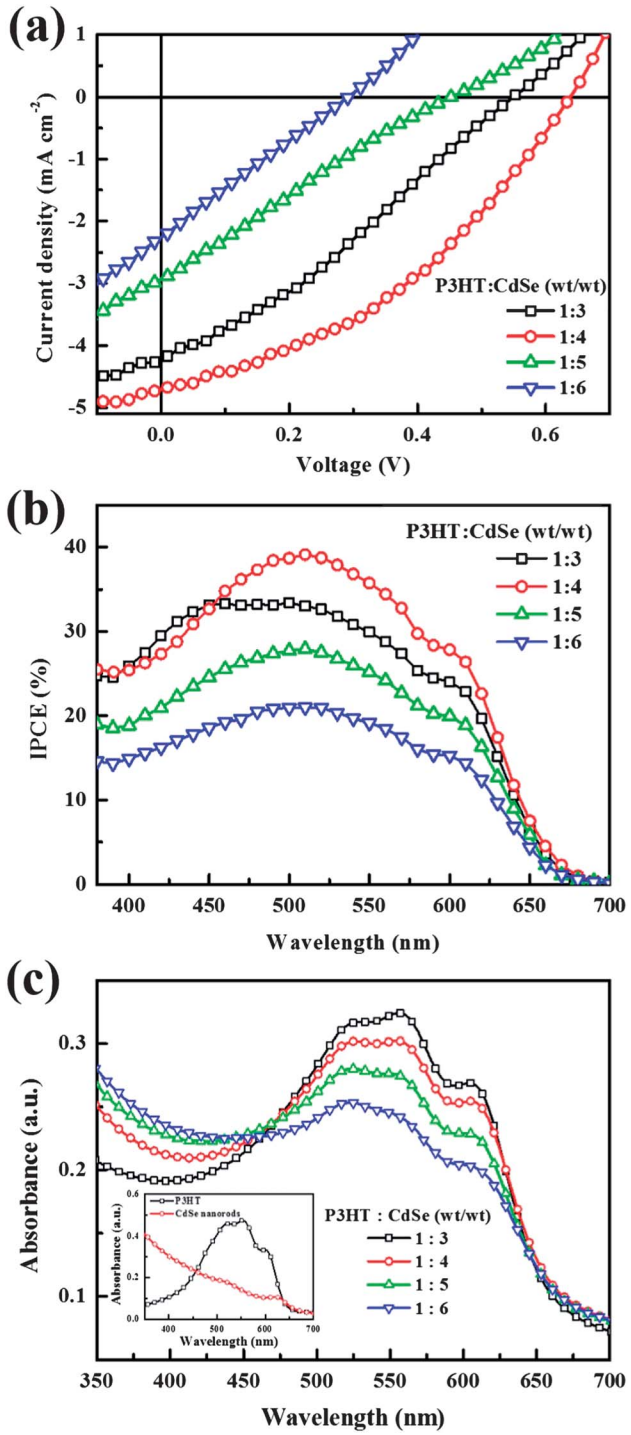

Fig. 5 (a) *J–V* curves, (b) IPCE spectra of inverted P3HT : CdSe hybrid solar cells with various compositions of P3HT : CdSe using the ZnO:Cs (Cs/Zn molar ratio = 0.094) electron transport layer. (c) UV-Vis absorption spectra of P3HT : CdSe hybrid thin films composed of various compositions of P3HT and CdSe on a quartz substrate after annealing at 120 °C. The inset corresponds to the UV-Vis spectra of neat P3HT and CdSe nanorods films.

inverted structure of the devices, the contribution of P3HT to the photocurrent generation was considerably higher than that of CdSe, which is verified by UV-Vis absorption spectra (see Fig. 5(c)).

To clarify the variation of device performance depending on the weight ratio of P3HT and CdSe, the CdSe to P3HT composition ratio at the top and bottom surfaces of spin-coated films was evaluated by XPS. Here, we used the atomic ratio of Cd in CdSe to S in P3HT. We prepared the films by spin-coating P3HT : CdSe solutions onto NaCl substrates and thermal annealing at 120 °C for 20 min. To characterize the Cd/S atomic ratio at the bottom of the P3HT : CdSe layer, the top of the P3HT : CdSe was coated with epoxy with a curing agent and cross-linked by heating at 60 °C for 12 h. Finally, the NaCl substrate was removed by dipping it in deionized water. Fig. 6(a) gives the Cd/S atomic ratio dependence on the weight ratios of P3HT and CdSe. All samples show higher Cd/S atomic ratios on the bottom surface compared with the top surface. With increasing CdSe concentration in the active layer, top contact of CdSe is increased. From this result, we can schematically draw vertically segregated distribution of P3HT and CdSe through the film thickness: more P3HT molecules are located near the top surface, while a large amount of CdSe exists near the bottom surface (Fig. 6(b)). This implies that a large amount of CdSe is needed in the normal structure of hybrid solar cells for efficient electron extraction to the top electrode. In contrast, the optimized performance could be obtained in inverted hybrid solar cells with much lower CdSe concentration. The device with 1 : 4 (wt/wt) P3HT : CdSe showed a better PCE than that with 1 : 3 (wt/wt) P3HT : CdSe due to sufficient CdSe interconnection for electron pathways. Above 1 : 5 (wt/wt) P3H : CdSe, the

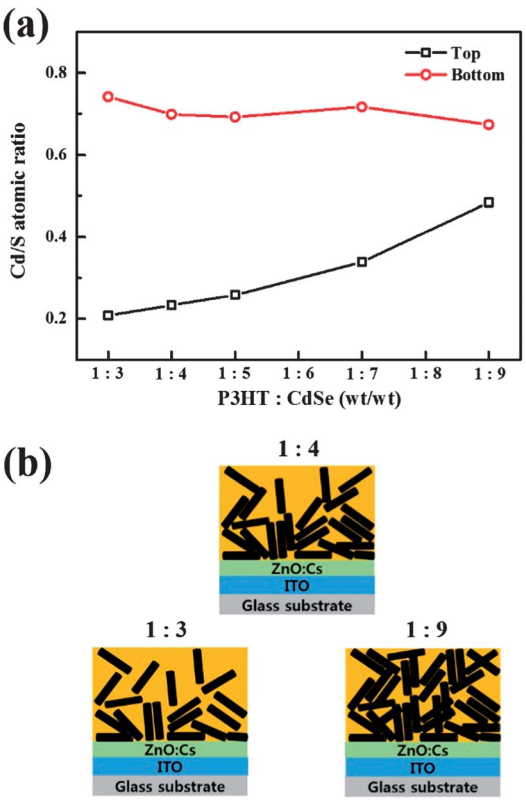

Fig. 6 (a) Cd/S atomic ratios of P3HT : CdSe active layers at the top and bottom measured by XPS and (b) schematic illustration of the vertical device structure.

concentration of P3HT on the top surface of an active layer is decreased. Because hole extraction through the P3HT is more restricted compared with that in the optimum device, the device has a lower current level and higher R_S.

Fig. 7(a) shows the *J–V* curves for normal and inverted hybrid solar cells. The normal hybrid solar cell consists of ITO/PEDOT:PSS/P3HT : CdSe/Al. The weight ratio of P3HT to CdSe was 1 : 9, which showed the best performance: a V_{OC} of 0.633 V, a J_{SC} of 4.4 mA cm^{-2}, and an FF of 46.6%; thus, a PCE of 1.30%. The inverted hybrid solar cell consists of ITO/ZnO:Cs(Cs/Zn molar ratio = 0.094)/P3HT : CdSe(1 : 4 weight ratio)/MoO_3/Ag. This device shows the best performance (1.14%), which was comparable to the PCE of the normal hybrid solar cell. The inset of Fig. 7(a) shows the IPCE spectra of normal and inverted hybrid solar cells. The normal device is most efficient near 400 nm corresponding to the absorption of CdSe, while the inverted device is most efficient near 525 nm, corresponding to absorption of P3HT, and both IPCEs reach 39%. P3HT has a strong absorption band between 450 and 650 nm, which complements low absorption of CdSe. Fig. 7(b) shows the stability test of the normal and inverted hybrid solar cells. The unencapsulated devices were stored under dark and ambient conditions and periodically tested over 168 hours. Although the PCE (1.30%) of the normal hybrid solar cell is slightly higher than that (1.14%) of the inverted hybrid solar cell, the former cell becomes very unstable in air, because the PCE was reduced to almost 0% in less than 24 h. The inverted hybrid solar cell, however, is much more stable in the air. Namely, over 70% of the original PCE of the devices was preserved even after 168 h of storage. This is because an air-stable inorganic ZnO:Cs layer was employed on the ITO glass substrate in the inverted structure instead of using the acidic and hygroscopic PEDOT:PSS layer in the normal structure.[30–33]

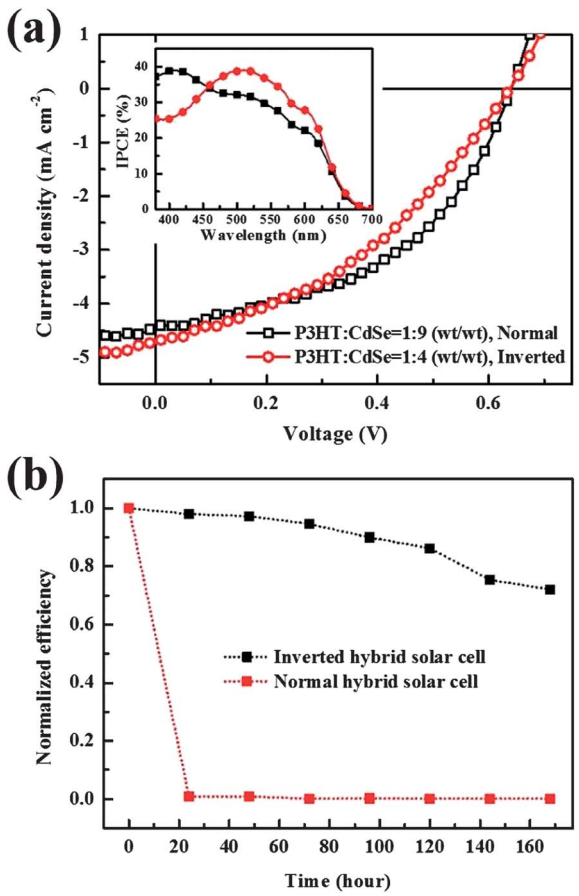

Fig. 7 (a) *J–V* curves and (b) the stability test of inverted and normal P3HT : CdSe hybrid solar cells. The inset corresponds to the IPCE spectra of normal and inverted hybrid solar cells.

Conclusions

We have studied the effect of the ZnO:Cs electron transport layer with various Cs/Zn molar ratios on the performance of the inverted structure of P3HT : CdSe hybrid solar cells. For inverted P3HT : CdSe (1 : 4 weight ratio) hybrid solar cells, the PCE is significantly improved from 0.43% for a device using pristine ZnO to 1.14% for another device using ZnO:Cs with a Cs/Zn molar ratio of 0.094. The increase in V_{OC} is mainly attributed to the shift of the conduction band edge of ZnO:Cs to match the LUMO of CdSe. The improved J_{SC} mainly stems from lowered R_S and more efficient electron extraction due to a better energy level match at the electron extraction contact. Moreover, vertically inhomogeneous distribution of P3HT and CdSe in the film, where CdSe is more abundant at the bottom surface, is suitable for electron extraction from CdSe in the active layer to ZnO:Cs and efficient hole extraction from P3HT in the active layer to the top electrode in the inverted structure of hybrid solar cells. The inverted structure of P3HT : CdSe hybrid solar cells showed very high air-stability because it does not use the PEDOT:PSS layer. Fabrication of the inverted hybrid solar cell with further improved PCE might be possible by using a low-band-gap p-type polymer capable of absorbing broad-wavelength light.

Acknowledgements

We acknowledge the support from the National Creative Research Initiative Program and the second stage of the BK21 Programs supported by the National Research Foundation of Korea (NRF). This work was also supported by a grant (Code no. 2011-0031639) from the Center for Advanced Soft Electronics under the Global Frontier Research Program of the Ministry of Science, ICT, and Future Planning, Korea.

Notes and references

1 W. U. Hyunh, J. J. Dittmer and A. P. Alivisatos, *Science*, 2002, **295**, 2425.
2 L.-S. Li, J. Hu, W. Yang and A. P. Alivisatos, *Nano Lett.*, 2001, **1**, 349.
3 A. P. Alivisatos, *Science*, 1996, **271**, 933.
4 L. Fang, J. Y. Park, Y. Cui, P. Alivisatos, J. Shcrier, B. Lee, L.-W. Wang and M. Sameron, *J. Chem. Phys.*, 2007, **127**, 184704.

5 H. Wei, H. Zhang, G. Jin, T. Na, G. Zhang, X. Zhang, Y. Wang, H. Sun, W. Tian and B. Yang, *Adv. Funct. Mater.*, 2013DOI: 10.1002/adfm.201300333.
6 B. Sun, H. J. Snaith, A. S. Dhoot, S. Westenhoff and N. C. Greenham, *J. Appl. Phys.*, 2005, **97**, 014914.
7 J. Seo, M. J. Cho, D. Lee, A. N. Cartwright and P. N. Prasad, *Adv. Mater.*, 2011, **23**, 3984.
8 S. Ren, L.-Y. Chang, S.-K. Lim, J. Zhao, M. Smith, N. Zhao, V. Bulovic, M. Bawendi and S. Gradecak, *Nano Lett.*, 2011, **11**, 3998.
9 Z. Chen, H. Zhang, X. Du, X. Cheng, X. Chen, Y. Jiang and B. Yang, *Energy Environ. Sci.*, 2013, **6**, 1597.
10 H. Wei, H. Sun, H. Zhang, W. Yu, F. Zhai, Z. Fan, W. Tian and B. Yang, *J. Mater. Chem.*, 2012, **22**, 9161.
11 H. Wei, H. Zhang, H. Sun, W. Yu, Y. Liu, Z. Chen, L. Cui, W. Tian and B. Yang, *J. Mater. Chem.*, 2012, **22**, 17827.
12 H. Wei, H. Zhang, H. Sun and B. Yang, *Nano Today*, 2012, **7**, 316.
13 Y. Liu, D. Yao, L. Shen, H. Zhang, X. Zhang and B. Yang, *J. Am. Chem. Soc.*, 2012, **134**, 7207.
14 M. Jørgensen, K. Norrman and F. C. Krebs, *Sol. Energy Mater. Sol. Cells*, 2008, **92**, 686.
15 Z. Chen, H. Zhang, W. Yu, Z. Li, J. Hou, H. Wei and B. Yang, *Adv. Energy Mater.*, 2013, **3**, 433.
16 S. Dowland, T. Lutz, A. Ward, S. P. King, A. Sudlow, M. S. Hill, K. C. Molloy and S. A. Haque, *Adv. Mater.*, 2011, **23**, 2739.
17 H.-C. Chen, C.-W. Lai, I.-C. Wu, H.-R. Pan, I.-W. P. Chen, Y.-K. Peng, C.-L. Liu, C.-H. Chen and P.-T. Chou, *Adv. Mater.*, 2011, **23**, 5451.
18 J. C. Hindson, Z. Saghi, J.-C. Hernandez-Garrido, P. A. Midgley and N. C. Greenham, *Nano Lett.*, 2011, **11**, 904.
19 D. Hwang, D. Y. Kim, S.-Y. Jang and D. Kim, *J. Mater. Chem. A*, 2013, **1**, 1228.
20 S. Kwon, H. C. Moon, K.-G. Lim, D. Bae, S. Jang, J. Shin, J. Park, T.-W. Lee and J. K. Kim, *J. Mater. Chem. A*, 2013, **1**, 2401.
21 H. C. Moon, A. Anthonysamy, Y. Lee and J. K. Kim, *Macromolecules*, 2010, **43**, 1747.
22 M. Jeffries-El, G. Sauve and R. D. McCullough, *Adv. Mater.*, 2004, **16**, 1017.
23 J. D. Servaites, S. Yeganeh, T. J. Marks and M. A. Ratner, *Adv. Funct. Mater.*, 2010, **20**, 97.
24 Z. Ma, Z. Tang, E. Wang, M. R. Andersson, O. Inganäs and F. Zhang, *J. Phys. Chem. C*, 2012, **116**, 24462.
25 S. Kwon, M. Shim, J. I. Lee, T.-W. Lee, K. W. Cho and J. K. Kim, *J. Mater. Chem.*, 2011, **21**, 12449.
26 Z.-Q. Xu, J.-P. Yang, F.-Z. Sun, S.-T. Lee, Y.-Q. Li and J.-X. Tang, *Org. Electron.*, 2012, **13**, 697.
27 B. R. Lee, H. Choi, J. S. Park, H. J. Lee, S. O. Kim, J. Y. Kim and M. H. Song, *J. Mater. Chem.*, 2011, **21**, 2051.
28 C.-R. Ho, M.-L. Tsai, H.-J. Jhuo, D.-H. Lien, C.-A. Lin, S.-H. Tsai, T.-C. Wei, K.-P. Huang, S.-A. Chen and J.-H. He, *Nanoscale*, 2013, **5**, 6350–6355.
29 M. J. Greaney, S. Das, D. H. Webber, S. E. Bradforth and R. L. Brutchey, *ACS Nano*, 2012, **6**, 4222.
30 K. Kawano, R. Pacios, D. Poplavskyy, J. Nelson, D. D. C. Bradley and J. R. Durrant, *Sol. Energy Mater. Sol. Cells*, 2006, **90**, 3520.
31 M. P. de Jong, L. J. van IJzendoom and M. J. A. de Voigt, *Appl. Phys. Lett.*, 2000, **77**, 2255.
32 K. W. Wong, H. L. Yip, Y. Luo, K. Y. Wong, W. M. Lau, K. H. Low, H. F. Chow, Z. Q. Gao, W. L. Yeung and C. C. Chang, *Appl. Phys. Lett.*, 2002, **80**, 2788.
33 E. Voroshazi, B. Verreet, A. Buri, R. Müller, D. D. Nuzzo and P. Heremans, *Org. Electron.*, 2011, **12**, 736.

